J|A|C|S
ARTICLES
Published on Web 09/02/2006

Synthesis, Reactivity, and DFT Studies of Tantalum Complexes Incorporating Diamido-*N*-heterocyclic Carbene Ligands. Facile Endocyclic C−H Bond Activation

Liam P. Spencer,[†] Chad Beddie,[‡] Michael B. Hall,*[,‡] and Michael D. Fryzuk*[,†]

Contribution from the Department of Chemistry, University of British Columbia, 2036 Main Mall, Vancouver, British Columbia, Canada, V6T 1Z1, and Department of Chemistry, Texas A&M University, College Station, Texas 77843

Received May 25, 2006; E-mail: fryzuk@chem.ubc.ca; hall@science.tamu.edu

Abstract: The syntheses of tantalum derivatives with the potentially tridentate diamido-*N*-heterocyclic carbene (NHC) ligand are described. Aminolysis and alkane elimination reactions with the diamine−NHC ligands, ^{Ar}[NCN]H$_2$ (where ^{Ar}[NCN]H$_2$ = (ArNHCH$_2$CH$_2$)$_2$(C$_3$N$_2$); Ar = Mes, *p*-Tol), provided complexes with a bidentate amide−amine donor configuration. Attempts to promote coordination of the remaining pendent amine donor were unsuccessful. Metathesis reactions with the dilithiated diamido−NHC ligand (^{Ar}[NCN]Li$_2$) and various Cl$_x$Ta(NR′$_2$)$_{5-x}$ precursors were successful and generated the desired octahedral ^{Ar}[NCN]TaCl$_x$(NR′$_2$)$_{3-x}$ complexes. Attempts to prepare trialkyl tantalum complexes by this methodology resulted in the formation of an unusual metallaaziridine derivative. DFT calculations on model complexes show that the strained metallaaziridine ring forms because it allows the remaining substituents to adopt preferable bonding positions. The calculations predict that the lowest energy pathway involves a tantalum alkylidene intermediate, which undergoes C−H bond activation α to the amido to form the metallaaziridine moiety. This mechanism was confirmed by examining the distribution of deuterium atoms in an experiment between ^{Mes}[NCN]Li$_2$ and Cl$_2$Ta(CD$_2$Ph)$_3$. The single-crystal X-ray structures of $^{p-Tol}$[NCNH]Ta(NMe$_2$)$_4$ (**3**), ^{Mes}[NCNH]Ta=CHPh(CH$_2$Ph)$_2$ (**4**), $^{p-Tol}$[NCN]Ta(NMe$_2$)$_3$ (**7**), ^{Mes}[NCCN]Ta(CH$_2$^{t}Bu)$_2$ (**11**), and ^{Mes}[NCCN]-TaCl(CH$_2$^{t}Bu) (**14**) are included.

Introduction

Designing homogeneous catalysts that are selective, display fast turnover rates, and are long-lived continues to be the goal of many research groups. Generally, the approach taken is to examine different kinds of ligand−metal combinations in an effort to find the one that provides catalysts that are efficient and robust.[1,2] The reason that a particular catalyst degrades over time can often be related to the ancillary ligand either dissociating or undergoing some side reaction that alters its binding mode. An obvious way to overcome dissociation is to examine multidentate ligands, which can help increase the stability of the complex.[3]

In terms of ancillary ligand design, research into the use of *N*-heterocyclic carbene (NHC) donors has been especially intense. Once considered academic curiosities, NHCs are now considered phosphine equivalents,[4] with the added feature that transition metal NHC-complexes show enhanced catalytic activity as compared to their phosphine analogues. Also, an important feature of NHCs is that they form remarkably stable metal−carbene bonds, which is an important aspect for robust catalyst design.[5−10]

While monodentate NHC ligands are becoming quite common, of increasing interest is the incorporation of NHCs into multidentate ligand arrays. There are a number of bidentate and tridentate ancillary ligands that contain one or two NHC units along with neutral or anionic donors.[11−16] Our research has been concerned with tridentate, formally dianionic ligands that incorporate NHCs as the central donor with two flanking amido units, which we denote as [NCN]. These ligands were specifically designed to coordinate to the early transition metals.

[†] University of British Columbia.
[‡] Texas A&M University.

(1) Gennari, C.; Piarulli, U. *Chem. Rev.* **2003**, *103*, 3071.
(2) Reetz, M. T. *Angew. Chem., Int. Ed.* **2001**, *40*, 284.
(3) Housecroft, C. E.; Sharpe, A. G. *Inorganic Chemistry*, 2nd ed.; Pearson Prentice Hall: Essex, 2005; p 183.
(4) Herrmann, W. A. *Angew. Chem., Int. Ed.* **2002**, *41*, 1290.
(5) Regitz, M. *Angew. Chem., Int. Ed. Engl.* **1996**, *35*, 725.
(6) Herrmann, W. A.; Kocher, C. *Angew. Chem., Int. Ed. Engl.* **1997**, *36*, 2162.
(7) Arduengo, A. J., III; Krafczyk, R. *Chem. Unserer Zeit* **1998**, *32*, 6.
(8) Arduengo, A. J., III *Acc. Chem. Res.* **1999**, *32*, 913.
(9) Dullius, J. E. L.; Suarez, P. A. Z.; Einloft, S.; de Souza, R. F.; Dupont, J.; Fischer, J.; De Cian, A. *Organometallics* **1998**, *17*, 815.
(10) Bourissou, D.; Guerret, O.; Gabbaie, F. P.; Bertrand, G. *Chem. Rev.* **2000**, *100*, 39.
(11) Chiu, P. L.; Lai, C.-L.; Chang, C.-F.; Hu, C.-H.; Lee, H. M. *Organometallics* **2005**, *24*, 6169.
(12) Lee, H. M.; Zeng, J. Y.; Hu, C.-H.; Lee, M.-T. *Inorg. Chem.* **2004**, *43*, 6822.
(13) Aihara, H.; Matsuo, T.; Kawaguchi, H. *J. Chem. Soc., Chem. Commun.* **2003**, 2204.
(14) Downing, S. P.; Danopoulos, A. A. *Organometallics* **2006**, *26*, 1337.
(15) Tsoureas, N.; Danopoulos, A. A.; Tulloch, A. A. D.; Light, M. E. *Organometallics* **2003**, *22*, 4750.
(16) Arnold, P. L.; Mungur, S. A.; Blake, A. J.; Wilson, C. *Angew. Chem., Int. Ed.* **2003**, *42*, 5981.

10.1021/ja063282x CCC: $33.50 © 2006 American Chemical Society

Earlier reports have been concerned with group 4 complexes, in particular with zirconium and hafnium alkyl complexes and their migratory insertion reactivity with carbon monoxide and isocyanide ligands.[17,18] Of particular note is that the [NCN] architecture renders the centrally disposed carbene donor stable toward dissociation[19] and not susceptible to migratory insertion processes that can alter the binding mode.[18]

In the present work, we have extended our studies to include the synthesis of tantalum−amide, −halide, and −alkyl compounds bearing an [NCN] ancillary ligand. In the case of tantalum alkyl compounds, endocyclic C−H bond activation of the tridentate ligand occurs irreversibly to yield a three-membered metallaaziridine moiety. DFT calculations were performed with model complexes to elucidate relative energies of intermediates in this reaction to shed insight on a possible mechanism for this transformation. As will be discussed, the tantalum−carbene bond length is very sensitive to the other ligands present in the coordination sphere.

Results and Discussion

The tridentate ligand precursors consisting of an NHC donor flanked by two amine arms having different substituents are shown below; the synthesis of these systems has already been described.[18]

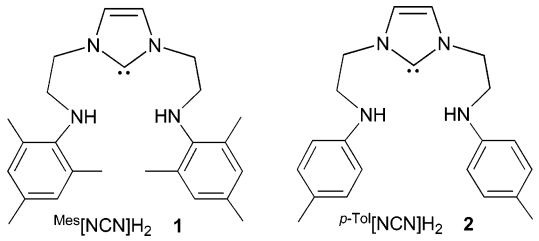

Recently, we reported that aminolysis reactions of ^{Mes}[NCN]-H_2 (**1**) and $M(NR_2)_4$ (M = Zr, Hf) are a convenient entry to ^{Ar}[NCN] group 4 metal complexes.[18] With this in mind, the reaction of *N*-mesityl precursor **1** with $Ta(NMe_2)_5$ was investigated. Disappointingly, there is no reaction even at elevated temperatures. Decreasing the steric bulk on the amide donors did however promote a reaction; the addition of $^{p-Tol}$[NCN]H_2 (**2**) to $Ta(NMe_2)_5$ in toluene yielded a product that did not show the expected C_{2v} symmetry in the ^{1}H NMR spectrum anticipated for $^{p-Tol}$[NCN]$Ta(NMe_2)_3$. Instead, a C_s symmetric species is observed in solution with four multiplets for the ethylene spacers, two doublets for the imidazole groups, two distinct sets of doublets typical of *para*-substituted aryl rings, two arylmethyl signals, and a broad resonance attributable to four $-NMe_2$ groups. Furthermore, a triplet at δ 3.32 is observed that can be ascribed to an amino −NH group. A weak downfield resonance is observed in the ^{13}C NMR spectrum at δ 198.5, typical of a metal−carbene carbon atom. These NMR data are consistent with partial aminolysis to generate one arm of the ligand coordinated along with the NHC and the remaining ligand arm dangling as the free amine, as shown in eq 1.

The solid-state molecular structure of $^{p-Tol}$[NCNH]$Ta(NMe_2)_4$ (**3**) is shown in Figure 1 and confirms the bidentate binding of

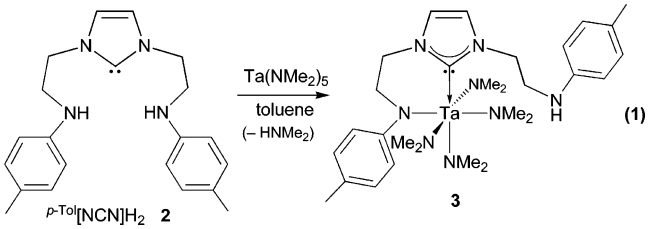

ancillary ligand. The ligand assumes an amide−amine donor configuration with respect to distorted octahedral geometry. The Ta1−C1 carbene bond length is 2.407(4) Å and represents to the best of our knowledge the first crystallographically characterized Ta−C NHC bond; other Ta−C bond lengths to sp^3 carbon centers are typically shorter at 2.2−2.3 Å. The Ta−N amido bond lengths are similar to other reported compounds.[20−24] Although introduction of the [NCN] ligand is incomplete, we were encouraged by the formation of a new Ta−C NHC bond. Unfortunately, all attempts to promote the coordination of the remaining pendent amine arm have been unsuccessful.

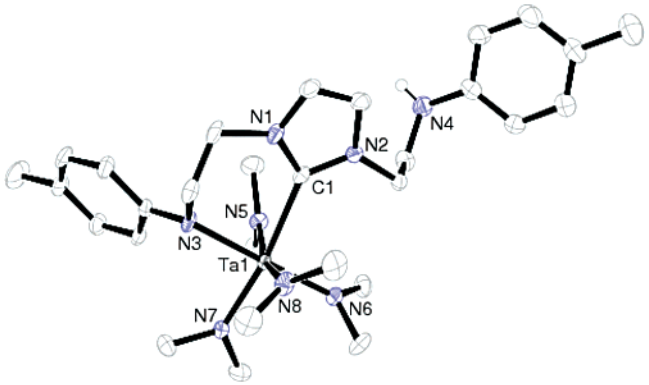

Figure 1. ORTEP view of $^{p-Tol}$[NCNH]$Ta(NMe_2)_4$ (**3**) depicted with 50% thermal ellipsoids; all hydrogen atoms attached to carbon have been omitted for clarity. Selected bond distances (Å) and angles (deg): Ta1−N8 2.050-(3), Ta1−N3 2.181(3), Ta1−C1 2.407(4), N6−Ta1−N3 178.48(11), N8−Ta1−N3 90.58(12), N3−Ta1−C1 80.14(11).

We have also shown that alkyl elimination reactions between **2** and $Zr(CH_2R)_4$ (R = $SiMe_3$, Ph) provide the desired dialkyl $^{p-Tol}$[NCN]$Zr(CH_2R)_2$ complexes.[17] A similar approach was examined with the *N*-mesityl precursor **1** and $Ta(CH_2Ph)_5$ (eq 2). The reaction proceeds immediately in toluene to give dark brown **4**, which displays a ^{1}H NMR spectrum consistent with C_s symmetry, similar to that observed for **3**. A bidentate interaction of the ancillary ligand is inferred on the basis of the low symmetry; unfortunately, the presence of the NH resonance was obscured. In addition, a resonance integrating to one proton is observed at δ 4.81 and correlates with a ^{13}C resonance located at δ 236.3 in the ^{13}C NMR spectrum; these data are diagnostic of a benzylidene moiety, Ta=CHPh. Presumably, benzylidene formation proceeds via the intermediacy of the unobserved tetraalkyl ^{Mes}[NCNH]$Ta(CH_2Ph)_4$ intermediate.[25] Interestingly, there is no change in the position of the ^{13}C Ta−carbene resonance (or that in **3**) in the presence of neat pyridine over a

(17) Spencer, L. P.; Winston, S.; Fryzuk, M. D. *Organometallics* **2004**, *23*, 3372.
(18) Spencer, L. P.; Fryzuk, M. D. *J. Organomet. Chem.* **2005**, *690*, 5788.
(19) Arnold, P. L.; Mungur, S. A.; Blake, A. J.; Wilson, C. *Angew. Chem., Int. Ed.* **2003**, *42*, 5981.
(20) Tanski, J. M.; Parkin, G. *Inorg. Chem.* **2003**, *42*, 264.
(21) Tin, M. K. T.; Yap, G. P. A.; Richeson, D. S. *Inorg. Chem.* **1999**, *38*, 998.
(22) Tin, M. K. T.; Yap, G. P. A.; Richeson, D. S. *Inorg. Chem.* **1998**, *37*, 6728.
(23) Guzei, I. A.; Yap, G. P. A.; Winter, C. H. *Inorg. Chem.* **1997**, *36*, 1738.
(24) Chisholm, M. H.; Huffman, J. C.; Tan, L.-S. *Inorg. Chem.* **1981**, *20*, 1859.
(25) Schrock, R. R. *Chem. Rev.* **2002**, *102*, 145.

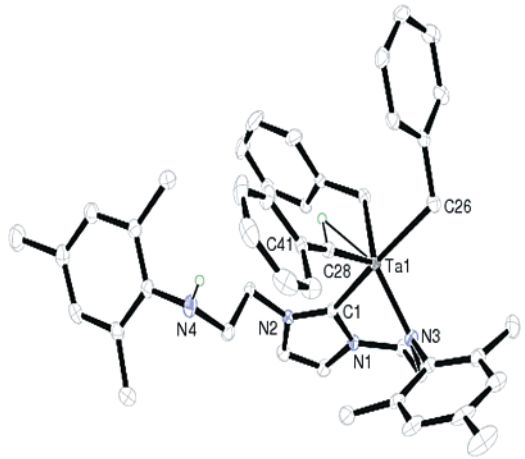

Figure 2. ORTEP view of ^{Mes}[NCNH]Ta=CHPh(CH_2Ph)$_2$ (**4**), depicted with 50% thermal ellipsoids; the hydrogen attached to C28 was isotropically refined, and all other hydrogen atoms attached to carbon have been omitted for clarity. Selected bond distances (Å) and angles (deg): Ta1−C28 1.940(3), Ta1−N3 2.011(2), Ta1−C26 2.243(3), Ta1−C27 2.259(3), Ta1−C1 2.290(3), N3−Ta1−C1 80.90(9), C41−C28−Ta1 164.5(2).

long period of time; this was unexpected in light of carbene dissociation reported in similar bidentate amido−carbene early transition metal and lanthanide complexes.[19] The formation of ^{Mes}[NCNH]Ta=CHPh(CH_2Ph)$_2$ (**4**) is shown in eq 2.

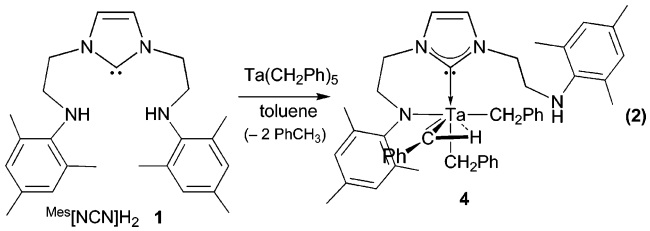

The molecular state structure of **4** is shown in Figure 2 and confirms the presence of a benzylidene moiety along with an amide−amine bidentate ligand configuration on a distorted square pyramidal metal center. The benzylidene moiety is clearly defined by the large Ta1−C28−C41 bond angle of 164.5(4)° and a short Ta1−C28 bond (1.940(4) Å); this Ta=C bond length is significantly shorter that the other two Ta−C benzyl bonds (∼2.26 Å) and is similar to previously described Ta−alkylidene complexes.[26] The Ta1−N3 amido bond length of 2.011(2) Å in **4** is similar to **3**, described above; the Ta1−C1 carbene bond distance of 2.290(3) Å is nearly 0.1 Å shorter that that found in **3** above. Attempts to promote coordination of the pendent amine arm by thermolysis reactions have proven futile, leading only to decomposition.

In light of the difficulty with aminolysis and alkane elimination reactions at Ta(V) centers, an alternative method was sought as a means to generate the desired tridentate coordination mode for this ligand system. Metathesis reactions with lithium amides have been used by many groups[27−29] including our own in the synthesis of early metal amido complexes.[30] Thus, the synthesis of the dilithium diamido NHC derivatives, ^{Ar}[NCN]Li_2, and their reactivity with suitable tantalum halide precursors were investigated. The addition of 2 equiv of BuLi to **1** and **2** yields ^{Mes}[NCN]Li_2 (**5**) and $^{p-Tol}$[NCN]Li_2 (**6**), respectively, in quantitative yield as insoluble powders (eq 3). The very poor solubility of these complexes has prevented any solid-state structural determinations; therefore, the structures shown are proposed on the basis of analogy to the arrangement of lithium ions observed in the dianionic diamidophosphine Li_2[NPN].[30,31] The ^{1}H NMR spectra in d_5-pyridine reveal broad resonances consistent with the proposed structures; the ^{1}H NMR spectrum of **6** is typical of both lithium species and reveals two broad multiplets for the ethylene spacers, one signal for aryl-methyl and imidazole environments, and two doublets for the *para*-substituted aryl ring. The ^{13}C NMR spectrum reveals a weak resonance at δ 189.9, similar to other lithium NHC compounds.[32] Additionally, a broad peak at δ 2.86 was observed in the ^{7}Li NMR spectrum.

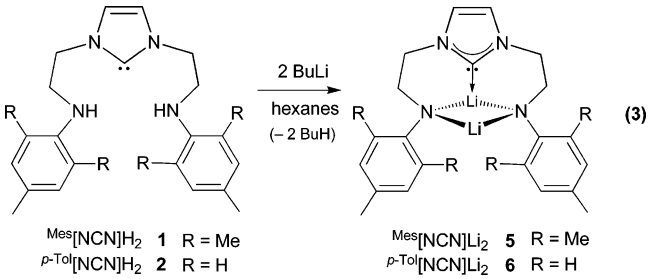

The metathesis reaction of **6** and $Cl_2Ta(NMe_2)_3$ proceeds at reduced temperature to yield $^{p-Tol}$[NCN]Ta(NMe_2)$_3$ (**7**) in good yield. A C_{2v} symmetric species is apparent from the ^{1}H NMR spectrum of **7** as two multiplets are observed for the equivalent ethylene spacers of the ligand backbone along with one set of resonances for each of the imidazole, aryl, and *para*-methyl aryl protons; there are two sets of resonances for the *N*-methyl protons of the NMe_2 groups in a ratio of 2:1 at δ 3.22 and 3.68. A weak resonance in the ^{13}C NMR spectrum was also observed at δ 186.7, indicative of a metal−carbene carbon atom.

Crystals suitable for X-ray diffraction were grown from toluene; the solid-state molecular structure is shown in Figure 3. The ligand adopts a meridional orientation with respect to a distorted octahedral metal center as evidenced by the cis oriented amido donors (N2−Ta1−N3 = 89.25(4)°) and N2−Ta1−N4 = 98.46(4)°). The molecule has a mirror plane that bisects the imidazole ring and lies along the C1−Ta1−N4 bond angle. The Ta−N amido bond lengths are similar to previously discussed complexes, **3** and **4**. However, the Ta1−C1 carbene bond distance of 2.365(6) Å is similar to that found in **3** but longer than observed in **4**.

Modification of the tantalum starting material serves as a useful entry into mixed amide−chloride metal complexes as outlined in Scheme 1. The reaction of **6** and $Cl_3Ta(NMe_2)_2$(THF) yields the expected product $^{p-Tol}$[NCN]TaCl(NMe_2)$_2$ (**8**). The ^{1}H NMR spectrum suggests a C_s symmetric species in solution on the basis of four sets of multiplets for the ethylene spacers and most noticeably three singlets integrating to six

(26) Messerle, L. W.; Jennische, P.; Schrock, R. R.; Stucky, G. *J. Am. Chem. Soc.* **1980**, *102*, 6744.
(27) Schrock, R. R.; Seidel, S. W.; Schrodi, Y.; Davis, W. D. *Organometallics* **1999**, *18*, 428.
(28) Clentsmith, G. K. B.; Bates, V. M. E.; Hitchcock, P. B.; Cloke, F. G. N. *J. Am. Chem. Soc.* **1999**, *121*, 10444.
(29) Laplaza, C. E.; Johnson, M. J. A.; Peters, J. C.; Odom, A. L.; Kim, E.; Cummins, C. C.; George, G. N.; Pickering, I. J. *J. Am. Chem. Soc.* **1996**, *118*, 8623.
(30) Fryzuk, M. D.; Johnson, S. A.; Patrick, B. O.; Albinati, A.; Mason, S. A.; Koetzle, T. F. *J. Am. Chem. Soc.* **2001**, *123*, 3960.
(31) MacLachlan, E. A.; Fryzuk, M. D. *Organometallics* **2005**, *24*, 1112.
(32) Mungur, S. A.; Liddle, S. T.; Wilson, C.; Sarsfield, M. J.; Arnold, P. L. *Chem. Commun.* **2004**, 2738.

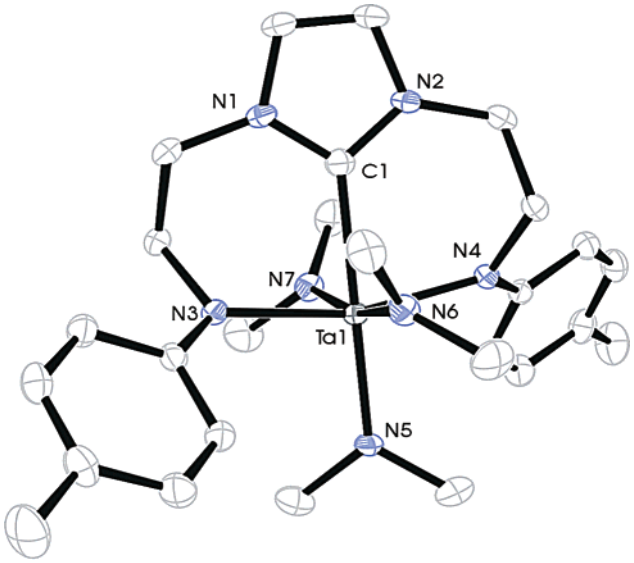

Figure 3. ORTEP view of $^{p-Tol}$[NCN]Ta(NMe$_2$)$_3$ (**7**), depicted with 50% thermal ellipsoids; all hydrogen atoms have been omitted for clarity. Selected bond distances (Å) and angles (deg): Ta1−N3 2.055(3), Ta1−N4 2.078(4), Ta1−N2 2.132(3), Ta1−C1 2.365(6), N3−Ta1−N2 89.25(13), N3−Ta1−C1 82.93(10), N2−Ta1−C1 81.54(9), N4−Ta1−C1 180.000(2).

Scheme 1. Synthesis of $^{p-Tol}$[NCN]Ta Amide Derivatives

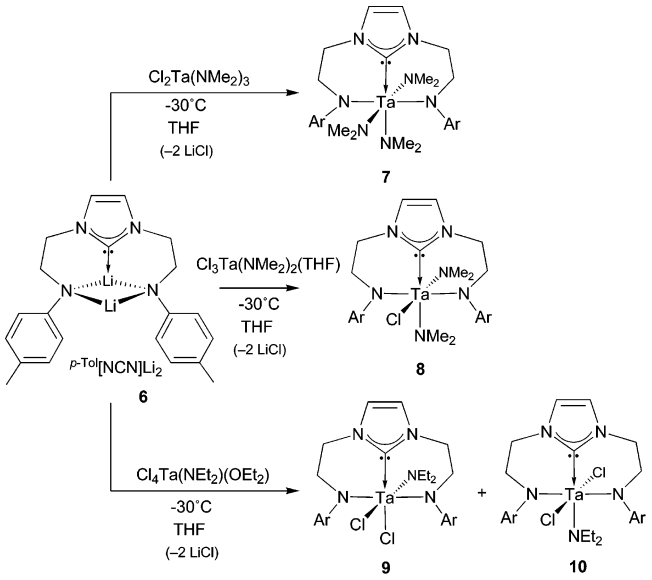

protons each. These latter data suggest a cis arrangement of −NMe$_2$ groups on the tantalum center. Although no single crystals of the product could be obtained, the NMR evidence for a cis structure is quite compelling given that trans oriented −NMe$_2$ groups would yield a species with C_{2v} symmetry in solution. A similar reaction with **6** and TaCl$_4$(NEt$_2$)(Et$_2$O) also yields the expected $^{p-Tol}$[NCN]TaCl$_2$(NEt$_2$) product. The ^{1}H NMR spectrum reveals the presence of two structural isomers in solution. The minor species possess C_s symmetry, a result that would be expected if there were cis chlorides on the tantalum center (**9**). The major species possesses C_{2v} symmetry, indicative of trans oriented chlorides on the metal center (**10**). Attempts to convert the amide groups of **7**−**10** to chlorides by reaction with Me$_3$SiCl have so far yielded a mixture of intractable materials as have the reactions of **5**,**6** with TaCl$_5$.

Given the success of coordinating the ^{Ar}[NCN] ligand to tantalum by metathesis reactions, the reactivity with mixed

Scheme 2. Synthesis of Cyclometalated [NCNC]Ta Alkyl Derivatives

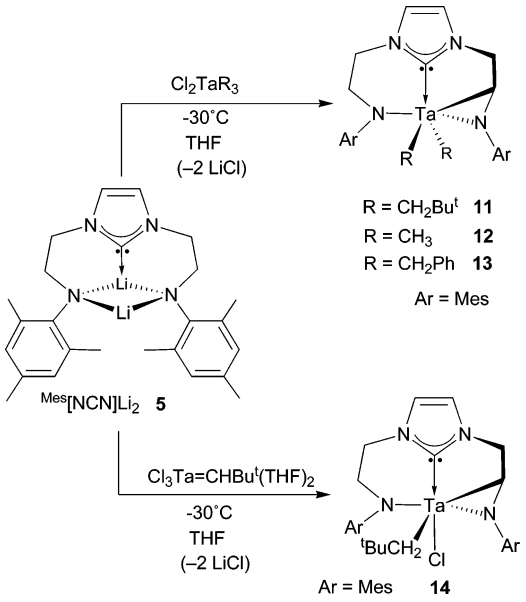

alkyl−chloro precursors of tantalum(V), Cl$_2$TaR$_3$ (R = CH$_2$^{t}Bu, Me, CH$_2$Ph), was examined (Scheme 2). The reaction of **5** with Cl$_2$Ta(CH$_2$^{t}Bu)$_3$ is representative and, like the amido precursors discussed above, proceeds rapidly at −30 °C in THF to give a brown solution. The ^{1}H NMR spectrum of the product reveals a complicated set of resonances indicative of a low-symmetry species. Not only are the imidazole-ring hydrogens inequivalent, but also the ethylene arms of the ligand backbone show sets of complex, coupled resonances, and the two remaining neopentyl groups are inequivalent as well. Clearly, a formulation based on the anticipated product ^{Mes}[NCN]Ta(CH$_2$^{t}Bu)$_3$ cannot be correct. The solid-state molecular structure of the isolated product was determined and is shown in Figure 4. Surprisingly, one of the six-membered chelate rings of the ligand backbone has undergone cyclometalation to form a set of adjacent five- and three-membered rings. The C−H bond activated ligand (denoted [NCCN]) in complex **11** adopts a facial orientation about a distorted pseudo trigonal bipyramidal metal

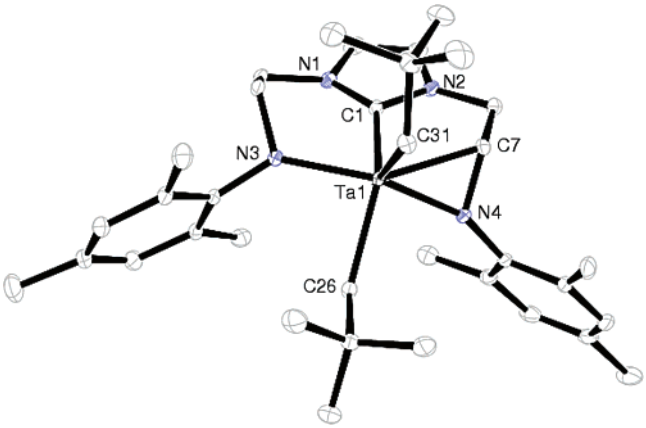

Figure 4. ORTEP view of ^{Mes}[NCCN]Ta(CH$_2$^{t}Bu)$_2$ (**11**), depicted with 50% thermal ellipsoids; all hydrogen atoms have been omitted for clarity. Selected bond distances (Å) and angles (deg): Ta1−N4 1.9877(15), Ta1−N3 2.0738(17), Ta1−C31 2.1833(17), Ta1−C1 2.2247(17), Ta1−C7 2.2257(19), Ta1−C26 2.255(2), N4−Ta1−N3 153.91(6), N4−Ta1−C1 89.46(6), N3−Ta1−C1 79.59(6), N4−Ta1−C7 39.37(6), N4−C7−Ta1 61.34(9), C7−N4−Ta1 79.29(10).

center. The bond angles defined by the Ta1−C7−N4 triangle are typical of a related, structurally characterized metallaaziridine tantalum complex derived from the 1,8-bis(isopropylamido)-naphthalene ligand;[33] however, in this latter case, the C−H activation occurs in an exocyclic manner. All of the Ta−C alkyl bonds of **11** are similar in length (∼2.24 Å) and are comparable to other reported Ta−C alkyl bond lengths.[26,30,34] Interestingly, the Ta1−C1 carbene bond length of 2.2247(17) Å is short as compared to the other complexes reported in this work (2.29−2.40 Å range). While part of the reason for this is likely due to the smaller five-membered chelate ring in **11** pulling the NHC closer to the tantalum center, as will be shown in the computational part of this paper, DFT analysis suggests that there is an electronic component for this shortened Ta1−C1 bond distance.

Intramolecular C−H bond activation of ligands in Ta complexes is relatively common,[35,36] particularly with amido-based systems.[33,34,37−40] Among these reports, the formation of metallaaziridine rings by exocyclic[33,39,40] C−H bond activation is known; the only example of an endocyclic[34] C−H bond activation involves a tripodal tris(aryloxy)amine system that activates next to the amine donor. In most examples, metallaaziridine ring formation appears to follow a σ-bond metathesis mechanism involving direct elimination of an alkane,[39] although in some cases the mechanism was not fully investigated.[34]

The unanticipated formation of the endocyclic [NCNC]Ta system by intramolecular C−H activation provided the incentive to examine this process computationally. Of particular interest was the fact the expected [NCN]TaR_3 species could not be observed.

Computational Analysis of Intramolecular C−H Bond Activation

Directed by literature findings, we explored two possible mechanisms for the formation of cyclometallated complexes.[39] Assuming that the first step of the reaction in Scheme 2 is formation of the trialkyl [NCN]TaR_3(R = $CH_2{}^tBu$, CH_3, CH_2-Ph), the ligand backbone β-H abstraction process that leads to the observed products **11**−**13** could occur by a one-step σ-bond metathesis pathway (Scheme 3, path 1), or by a two-step pathway that involves α-H abstraction to generate a [NCN]Ta=CHR′(R) alkylidene intermediate, followed by alkylidene-mediated C−H activation of the ligand backbone (Scheme 3, path 2).[39] As there is precedent for both path 1[35,37−39] and path 2[35] in organotantalum chemistry, we sought to determine which pathway is operational in the [NCN]Ta complexes using density functional theory.

The first step of the theoretical investigation was to construct a computational model of the experimental ligand that maintains

Scheme 3. Potential Pathways for Ligand β-H Abstraction

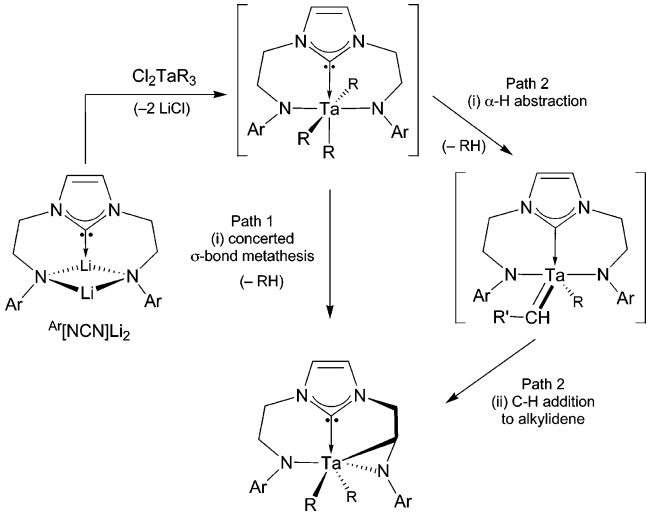

Chart 1. Computational Model of the [NCN] Ligand

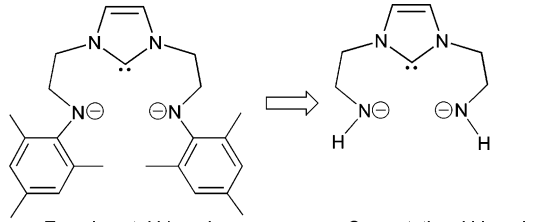

the diamido *N*-heterocyclic carbene framework of the ligand while minimizing the computational demands.[41] To this end, we chose to investigate the formation of the dimethyl tantalum complex (**12**) using a model in which the aryl groups on the MesNCN ligand were replaced with hydrogen atoms (Chart 1).

Using the model from Chart 1 and the B3LYP/BS1 level of theory, the mechanism of metallaaziridine formation from the trimethyl starting complex was investigated by calculating the structures and energies of intermediates and transition state structures along the σ-bond metathesis pathway (Scheme 3, path 1) and the two-step α-H abstraction/alkylidene-mediated C−H activation pathway (Scheme 3, path 2). The gas-phase relative free energies of the intermediates and transition state structures along the two pathways are presented in Table 1. The trimethyl complex HNCNTaMe_3 serves as a starting point for both paths 1 and 2; therefore the structures and energies of several conformers of the trimethyl tantalum complex were calculated. The lowest-energy structure of HNCNTaMe_3 (**A**, Figure 5) was used as a starting point for both ligand activation pathways.

In the calculated σ-bond metathesis pathway (Scheme 4), the lowest energy (unless otherwise noted, the energies in the text and schemes are free energies) trimethyl complex (**A**, $\Delta G°$ = 0.0 kcal/mol) is converted to a methane adduct of the ligand activated metallaziridine dimethyl complex (**B**, −7.9 kcal/mol), via the σ-bond metathesis transition state (**TS-A-B**, 49.6 kcal/mol). The calculated structures of **A**, **TS-A-B**, and **B** are provided in Figure 5. In the transition state **TS-A-B**, the breaking Ta−C bond distance is 2.96 Å, while the forming and breaking C−H bond distances are 1.36 and 1.47 Å, respectively. The

(33) Bazinet, P.; Yap, G. P. A.; Richeson, D. S. *Organometallics* **2001**, *20*, 4129.
(34) Groysman, S.; Goldberg, I.; Kol, M.; Genizi, E.; Goldschmidt, Z. *Organometallics* **2004**, *23*, 1880.
(35) Chamberlain, L. R.; Rothwell, I. P.; Huffman, J. C. *J. Am. Chem. Soc.* **1986**, *108*, 1502.
(36) Chamberlain, L. R.; Kerschner, J. L.; Rothwell, A. P.; Rothwell, I. P.; Huffman, J. C. *J. Am. Chem. Soc.* **1987**, *109*, 6471.
(37) Freundlich, J. S.; Schrock, R. R.; Davis, W. M. *J. Am. Chem. Soc.* **1996**, *118*, 3643.
(38) Freundlich, J. S.; Schrock, R. R.; Davis, W. M. *Organometallics* **1996**, *15*, 2777.
(39) Abbenhuis, H. C. L.; Van Belzen, R.; Grove, D. M.; Klomp, A. J. A.; Van Mier, G. P. M.; Spek, A. L.; Van Koten, G. *Organometallics* **1993**, *12*, 210.
(40) de Castro, I.; Galakhov, M. V.; Gomez, M.; Gomez-Sal, P.; Royo, P. *Organometallics* **1996**, *15*, 1362.
(41) Beddie, C.; Webster, C. E.; Hall, M. B. *Dalton Trans.* **2005**, 3542.

Table 1. Gas-Phase Relative Energies (kcal/mol) of the Intermediates and Transition States in Path 2 α-H Abstraction Followed by Alkylidene-Mediated C−H Bond Activation

structure	ΔE_e[a]	ΔE_0[b]	ΔH°[c]	ΔG°[d]
		Path 1		
A	0.00	0.0	0.0	0.0
TS-A-B	55.33	49.7	49.9	49.6
B	1.99	−1.3	0.6	−7.9
C + CH_4	2.36	−1.1	−0.2	−10.5
TSC-D + CH_4	2.89	−1.0	−0.4	−10.4
D + CH_4	−5.85	−9.3	−8.4	−18.6
		Path 2		
A	0.00	0.0	0.0	0.0
TSA-E + CH_4	38.30	36.0	35.6	36.4
E + CH_4	−1.90	−4.7	−2.8	−10.3
F + CH_4	−1.56	−4.8	−3.6	−14.8
TSF-G + CH_4	8.09	4.8	5.4	−4.3
G + CH_4	−0.01	−3.0	−2.1	−12.5
TSG-H + CH_4	9.69	6.3	7.0	−3.1
H + CH_4	5.67	2.7	3.7	−7.3
TSH-I + CH_4	6.35	2.9	3.6	−6.5
I + CH_4	6.20	3.0	4.0	−6.7
TSI-J + CH_4	7.65	3.7	4.6	−5.7
J + CH_4	7.63	3.8	5.2	−7.0
TSJ-D + CH_4	31.43	25.8	26.2	17.3
D + CH_4	−5.85	−9.3	−8.4	−18.6

[a] Based on the gas-phase relative electronic energy of **A** set to 0.00 kcal/mol. [b] Based on the gas-phase relative zero-point corrected energy of **A** set to 0.0 kcal/mol. [c] Based on the gas-phase relative enthalpy of **A** set to 0.0 kcal/mol. [d] Based on the gas-phase relative free energy of **A** set to 0.0 kcal/mol.

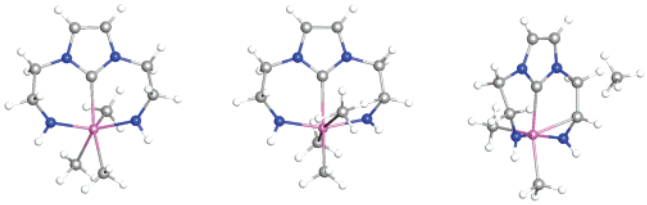

Figure 5. JIMP pictures of the one-step σ-bond metathesis pathway.

Ta−H distance in **TS-A-B** is 2.79 Å, which indicates that there is very little interaction between the migrating hydrogen and the tantalum center in this transition state. Separating the weakly bound methane from the methane adduct complex **B** generates the metallaaziridine complex **C** (−10.5 kcal/mol). The metallaaziridine complex **C** is able to change conformations to the most stable metallaaziridine complex **D** via the low barrier isomerization transition state (**TS-C-D**, −10.4 kcal/mol). Overall the reaction is exergonic, with the free energy of the metallaziridine **D** and CH_4 products being 18.6 kcal/mol lower in energy than the starting trimethyl complex **A**. However, the high energy point on this pathway, the transition state **TS-A-B**, is 49.6 kcal/mol higher in energy than the starting trimethyl complex **A**, which is too large of an energy difference between the starting complex and the transition state for this transformation to occur readily without heating the solution to elevated temperatures, and thus indicates this pathway may not be operating under the experimental conditions employed in this study.

In the calculated two-step pathway for metallaziridine formation (Scheme 5), in which α-H abstraction is followed by alkylidene-mediated C−H activation, the starting trimethyl complex (**A**, 0.0 kcal/mol) is initially converted to the methane-adduct methylidene−methyl complex (**E**, −10.3 kcal/mol) via the α-H abstraction transition state (**TS-A-E**, 36.4 kcal/mol) (Figure 6). Separating methane from the adduct-complex yields the methylidene−methyl complex and free methane (**F** + CH_4, −14.8 kcal/mol). Thus, the α-H abstraction sequence (**A** → **TS-A-E** → **E** → **F** + CH_4) is an energetically favorable process and the α-H abstraction transition state (**TS-A-E**) is 36.4 kcal/mol higher in energy than the starting trimethyl complex **A**, thus indicating that α-H abstraction is energetically favored over σ-bond metathesis for the trimethyl complex **A** by 13.5 kcal/mol.

A series of low energy rearrangements (**F** → **TS-F-G** → **G** → **TS-G-H** → **H** → **TS-H-I** → **I** → **TS-I-J** → **J**) positions the CH_2CH_2 carbene−amido linker in the proper position for alkylidene-mediated C−H activation of the ligand backbone. In the ligand C−H bond activation process, the methylidene unit of the rearranged methylidene−methyl complex (**J**, −7.0 kcal/mol) abstracts a proton from the ligand backbone via the alkylidene-mediated C−H activation transition state (**TS-J-D**, 17.3 kcal/mol) to yield the ligand activated metallaziridine product **D** (Figure 7). Overall, the final products **D** and CH_4 are lower in energy than all of the methylidene−methyl complexes (**F**−**J**), thus indicating that the metallaaziridine complex and CH_4 are the favored products for methane elimination from the trimethyl complex **A** in agreement with the experimental observations. In addition, the energy difference between the lowest energy methylidene−methyl complex (**F**) and the alkylidene-mediated C−H activation transition state (**TS-H-D**) is 32.1 kcal/mol, which indicates that the alkylidene-mediated C−H bond activation occurs more readily than the initial α-H abstraction step. It should also be noted that the barrier for the reaction to proceed in the reverse direction from lowest energy methylidene−methyl complex (**F**), that is, the energy difference between **F** and CH_4 and the α-H abstraction transition state (**TS-A-E**), is 51.2 kcal/mol, which suggests that endocyclic C−H activation of the ligand backbone is highly favored over C−H activation of alkanes in solution.

In addition to studying the mechanism of the ligand activation, part of the motivation for the DFT investigation was to address the question, why are the ligand activated metallaaziridine products formed instead of the trialkyl derivatives? For our model complexes, the metallaaziridine product **D** and separated CH_4 are favored relative to the trimethyl complex **A** in terms of both enthalpy and entropy (Table 1). Although we expected that formation of two molecules (**D** + CH_4) instead of one molecule (**A**) would be entropically favored, it was not obvious why the metallaaziridine product **D** and CH_4 were enthalpically favored over the trimethyl complex **A**, especially because **D** contains a three-membered ring, which is a potential source of ring strain.

An examination of the bond lengths and angles in the trimethyl complex **A** (Figure 8) and the metallaaziridine product **D** (Figure 9) revealed several features that contribute to **D** and CH_4 being enthalpically favored relative to **A**: (1) The Ta−carbene bond is much shorter in **D** (2.248 Å) than in **A** (2.381 Å), indicative of a much stronger bond. (2) The Ta−CH_3 bonds in **D** (2.173 and 2.219 Å) are shorter than the Ta−CH_3 bonds in **A** (2.238, 2.248, and 2.252 Å). (3) The Ta−N bonds in **D** (1.982 and 2.065 Å) are, on average, shorter than the Ta−N bonds in **A** (2.020 and 2.053 Å). Furthermore, the ring strain due to the metallaaziridine fragment in complex **D** is reduced

Scheme 4. Relative Free Energies of the Intermediates and Transition States in a Potential σ-Bond Metathesis Mechanism[a]

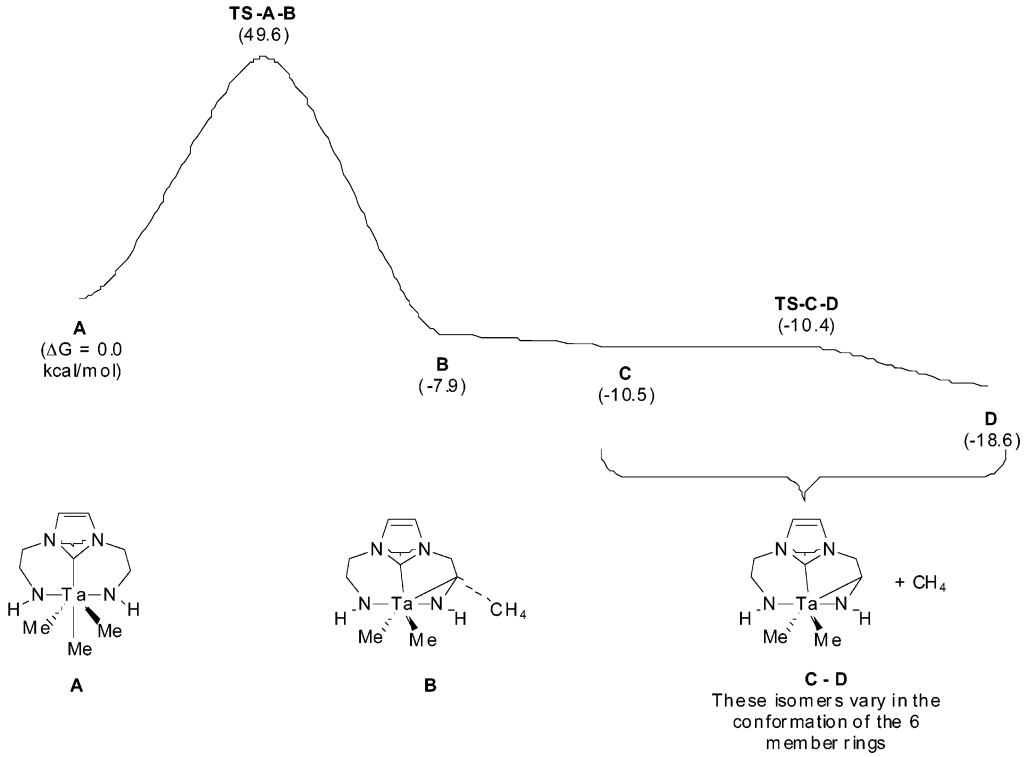

[a] Gas-phase relative free energies at the B3LYP/BS1 level of theory based on the energy of **A** set to 0.0 kcal/mol are provided in parentheses in kcal/mol. Electronic energies, zero-point corrected energies, enthalpies, and free energies are provided in Table 1.

Scheme 5. Relative Free Energies of the Intermediates and Transition States in a Potential Two-Step α-H Abstraction/Alkylidene-Mediated C−H Activation Mechanism[a]

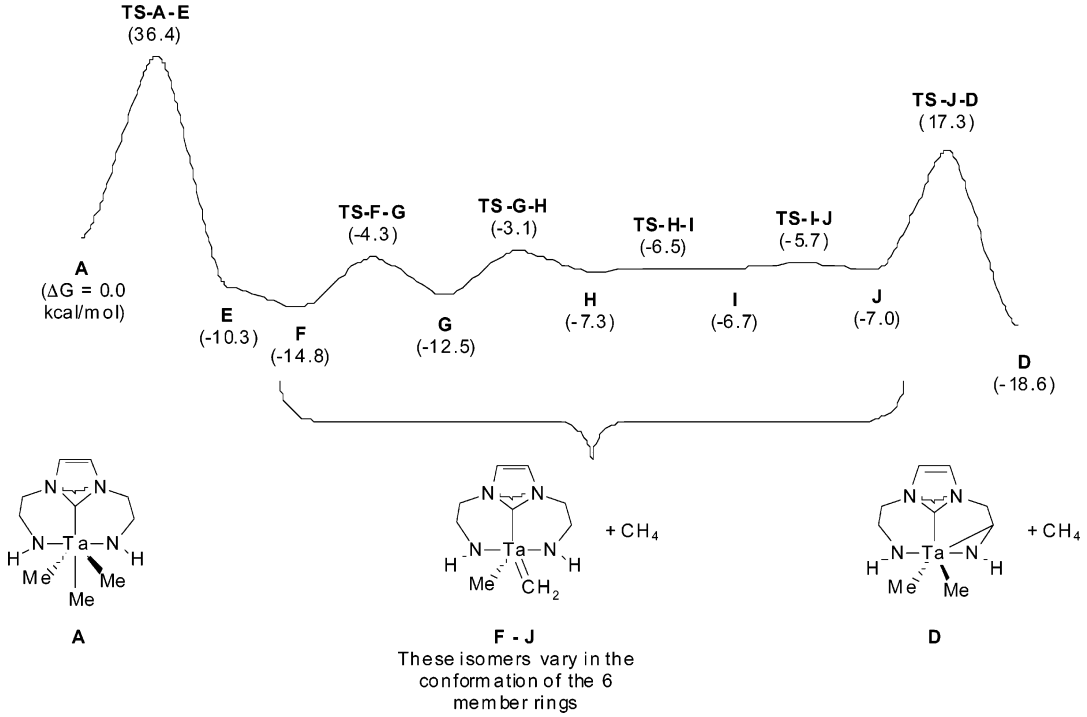

[a] Gas-phase relative free energies at the B3LYP/BS1 level of theory based on the energy of **A** set to 0.0 kcal/mol are provided in parentheses in kcal/mol. Electronic energies, zero-point corrected energies, enthalpies, and free energies are provided in Table 1

relative to the strain in organic three-membered rings because **D** can be viewed as a six-coordinate d^0 Ta complex in which Ta−L σ-bonding occurs through ligand orbital interactions with Ta sd^5 hybrids. In six coordinate, d^0 early transition metal complexes such as WH_6, formation of localized, electron pair bonds draws from all s and d orbitals to form six sd^5 hybrids,

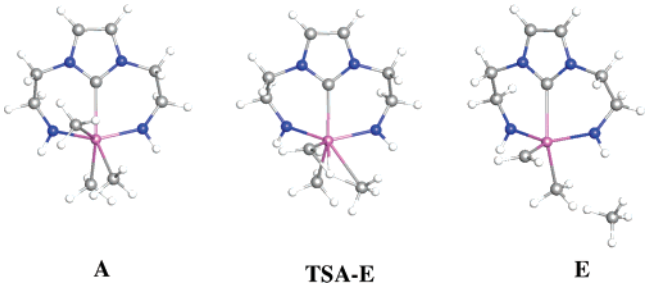

Figure 6. JIMP pictures of α-H abstraction by a methyl group to generate a [NCN]Ta(═CHR′)R alkylidene intermediate.

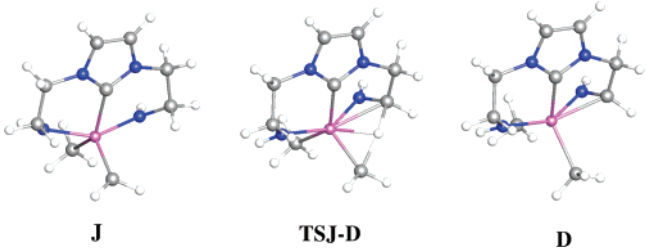

Figure 7. JIMP pictures of alkylidene-mediated C−H activation of the ligand backbone.

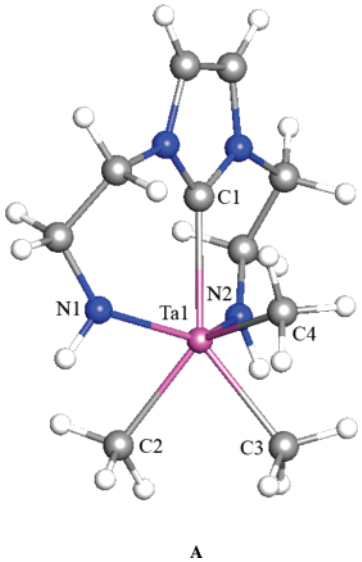

A

Figure 8. JIMP view of trimethyl **A**. Selected bond distances (Å) and angles (deg): Ta1−C1 2.381, Ta1−C2 2.252, Ta1−C3 2.248, Ta1−C4 2.238, Ta1−N1 2.053, Ta1−N2 2.020, C1−Ta1−C2 139.6, C1−Ta1−C3 142.0, C2−Ta1−C3 76.4.

which have energy minima at angles of 63° and 117°.[42,43] The calculated C4−Ta1−N2 angle in the metallaaziridine ring of **D** is 38.2°, which represents less than a 25° distortion from the smaller angle energy minima.

In addition, formation of the metallaaziridine ring in **D** forces the close proximity of two Ta substituents, which provides more space around the Ta center for the remaining substituents to adopt more favorable bonding positions. Natural Bond Orbital (NBO)[44,45] analyses of the trimethyl complex **A**, and the metallaaziridine product **D**, indicate that shortening of the Ta−

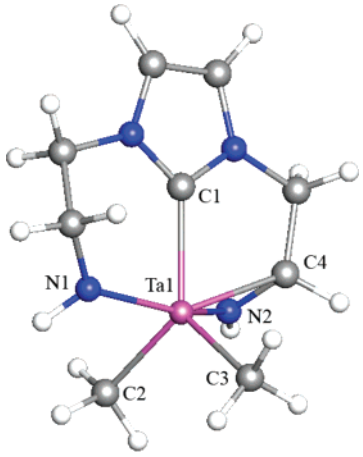

Figure 9. JIMP view of metallaaziridine **D**. Selected bond distances (Å) and angles (deg): Ta1−C1 2.248, Ta1−C2 2.219, Ta1−C3 2.173, Ta1−C4 2.257, Ta1−N1 2.065, Ta1−N2 1.982, C1−Ta1−C2 130.5, C1−Ta1−C3 122.7, C2−Ta1−C3 106.1, C4−Ta1−N2 38.2.

Table 2. NBO Occupancies of Bonding and Antibonding Orbitals in the Trimethyl Complex **A** and the Metallaaziridine Complex **D**

	A	D
Ta1−C1 σ	1.853	1.933
Ta1−X2 σ	1.833	1.946
Ta1−X3 σ	1.795	1.892
Ta1−X1 σ^*	0.168	0.091
Ta1−C2 σ^*	0.126	0.094
Ta1−C3 σ^*	0.129	0.103

Table 3. Important Second-Order Perturbation Theory Analysis of NBO Donor−Acceptor Interactions ΔE_{ij} (kcal/mol) That Contribute to Shorter Ta−Carbene and Ta−Me Bonds in the Metallaaziridine Product **D** Relative to the Trimethyl Complex **A**

		ΔE_{ij} (kcal/mol)	
NBO donor orbital (*i*)	NBO acceptor orbital (*j*)	A	D
Ta1−C1 σ	Ta1−X2 σ^*	26.13	1.02
Ta1−C1 σ	Ta1−X3 σ^*	31.50	2.64
Ta1−C2 σ	Ta1−X1 σ^*	38.32	1.81
Ta1−C3 σ	Ta1−X1 σ^*	54.62	3.02

carbene and Ta−Me bonds in **D** relative to **A** results from changes in the occupancy of the σ-bonding and σ^*-antibonding orbitals. The occupancies of the Ta−carbene and Ta−Me_3 σ-bonding orbitals in **D** are higher than the occupancies of the corresponding σ-bonding orbitals in **A**, while the occupancies of the Ta−carbene and Ta−Me_3 σ^*-antibonding orbitals in **D** are lower than the occupancies of the corresponding σ-bonding orbitals in **A** (Table 2).

Examination of the second-order perturbation theory analysis of the NBO orbitals of **A** reveals the origin of the differences in the orbital occupancies between **A** and **D** (Table 3). Strong donation from the σ-bonding orbitals to the trans Ta−C σ^* orbitals (Table 3, Figure 10) is shown by the large interaction terms for **A**. It should be noted that in **D**, the corresponding donation from the Ta−C σ-bonding orbitals to the Ta−C σ^* orbitals is significantly reduced (Table 3, Figure 11) because the more favorable C1−Ta−Me bond angles of **D** can avoid the mixing of bonding and antibonding orbitals observed in **A**. Thus, it appears that formation of the metallaaziridine ring is a key component that allows the remaining methyl and carbene substituents in **D** to adopt preferable bonding positions.

The other factor that causes the Ta−carbene distance to be shorter in the metallaaziridine complex **D** than in the trimethyl

(42) Bayse, C. A.; Hall, M. B. *J. Am. Chem. Soc.* **1999**, *121*, 1348.
(43) Landis, C. L.; Cleveland, T.; Firman, T. K. *J. Am. Chem. Soc.* **1995**, *11*, 1859.
(44) Reed, A. E.; Curtiss, L. A.; Weinhold, F. *Chem. Rev.* **1988**, *88*, 899.
(45) Weinhold, F.; Landis, C. R. *Valency and Bonding: A Natural Bond Orbital Donor-Acceptor Perspective*; Cambridge University Press: New York, 2005.

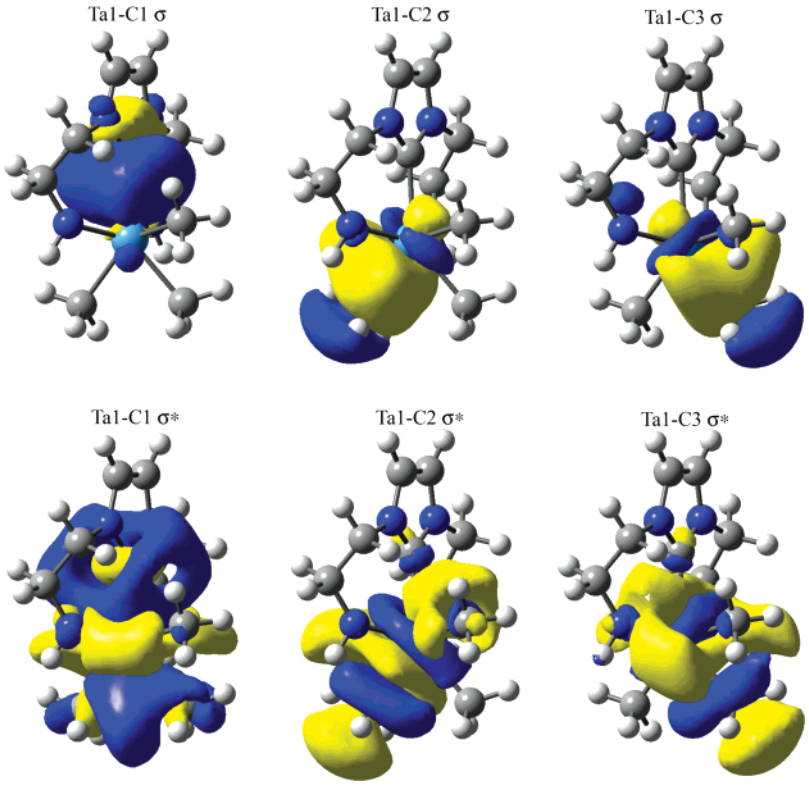

Figure 10. Gaussview representations of selected NBO bonding and antibonding orbitals in the trimethyl complex **A**.

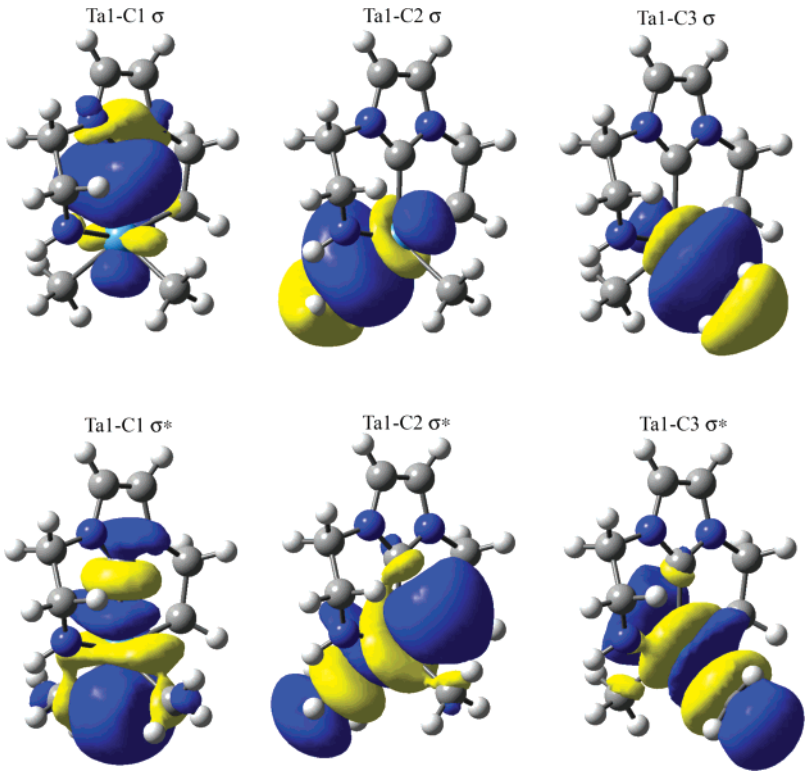

Figure 11. Gaussview representations of selected NBO bonding and antibonding orbitals in the metallaaziridine complex **D**.

complex **A** is the formation of the five-membered ring. To gauge how much of the shortening of the Ta−carbene bond in **D** relative to **A** is a result of the five-membered ring pulling the carbene toward the Ta-center, calculations were conducted on model complexes in which atoms linking the carbene unit to the amido donors were removed. In the first calculation, both CH_2CH_2 linkages in **A** were removed and replaced with H atoms to generate $(H_4N_2C_3)Ta(NH_2)_2(Me)_3$, **A′** (Figure 12). Optimization of **A′** resulted in a Ta−carbene bond length of 2.378 Å, which is only 0.003 Å shorter than for **A**, and indicates that the two six-membered rings do not significantly influence the Ta−carbene distance. In the second calculation, the CH_2CH_2 linkage

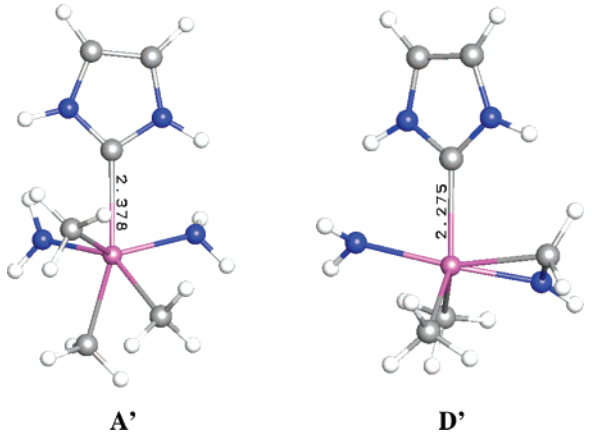

Figure 12. JIMP Pictures of **A′** and **D′**.

between the carbene and amido units, and the CH_2 linkage between the carbene and the metallaaziridine ring, were removed to generate $(H_4N_2C_3)Ta(NH_2)(NHCH_2)(Me)_2$, **D′** (Figure 12). The optimized Ta−carbene distance in **D′** is 2.275 Å, which is 0.027 Å longer than is observed in **D**. Thus, the calculations suggest that approximately 20% of the Ta−carbene bond shortening observed in **D** can be attributed to the five-membered ring pulling the carbene toward the Ta-center, while the remaining shortening can be attributed to electronic effects brought upon by the formation of the metallaaziridine ring (vide ante).

Experimental Verification of DFT Conclusions

Based on the computational support for the intermediacy of a tantalum alkylidene in the endocyclic C−H activation process, the synthesis of a bona fide ^{Ar}[NCN] tantalum alkylidene complex was attempted. Beginning with $Cl_3Ta{=}CH^tBu(THF)_2$, the reaction with **5** proceeds directly to the cyclometalated complex **14** in good yield (Scheme 2). Examination of this reaction by NMR spectroscopy reveals 2,2-dimethylpropane formation and no observable intermediates. An X-ray diffraction experiment was performed on crystals grown from Et_2O and reveals an endocyclic C−H bond activated complex with structural characteristics similar to those of the bis(neopentyl) complex **11** (Figure 13). Clearly, there is no alkylidene present as the Ta−C alkyl bonds from both complexes are of comparable length: Ta1−C26 is 2.244(4) Å in **14** similar to Ta1−C26 of 2.255(2) Å and Ta1−C31 of 2.1833(17) Å in **11**. Also evident is shortened Ta−carbene bond length in **14**; a Ta1−C1 bond distance of 2.241(4) Å is comparable to that found in **11** and consistent with the notion of the cyclometalated carbon facilitating stronger NHC−Ta bonding.

Although these experimental results cannot confirm the presence of an alkylidene intermediate in the decomposition of ^{Ar}[NCN]Ta(alkyl)$_3$ complexes, they infer that an alkylidene species can undergo rapid amido C−H bond activation. More definitive proof of the mechanism postulated by DFT calculations is observed in NMR deuterium experiments (Scheme 6). Utilizing $Cl_2Ta(CD_2Ph)_3$ as a starting material, we can examine the proton distribution in the final C−H bond activated product. If the mechanism proceeds as suggested by calculations, a proton from the ethylene spacer would transfer to an intermediate Ta=CDPh fragment to yield a Ta*CH*(D)Ph moiety. If a concerted σ-bond metathesis was the operant mechanism, this reaction

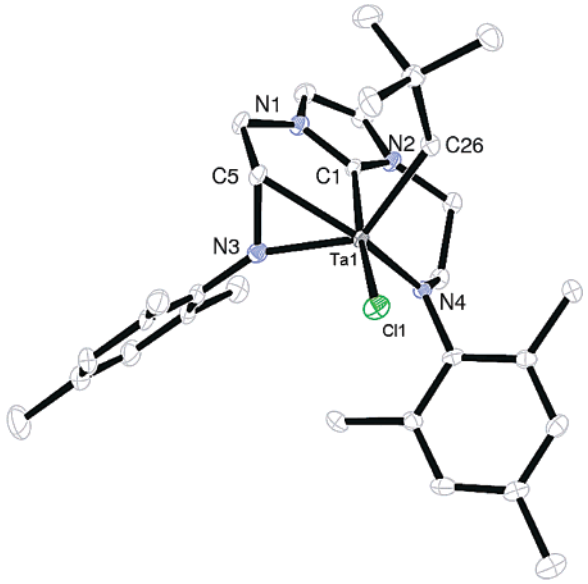

Figure 13. ORTEP view of ^{Mes}[NCCN]TaCl($CH_2{}^tBu$) (**14**), depicted with 50% thermal ellipsoids; all hydrogen atoms have been omitted for clarity. Selected bond distances (Å) and angles (deg): Ta1−N3 1.967(4), Ta1−N4 2.010(3), Ta1−C5 2.216(4), Ta1−C26 2.224(4), Ta1−C1 2.241(4), Ta1−Cl1 2.3996(11), N3−Ta1−N4 115.35(15), N3−Ta1−C5 39.64(16), N3−Ta1−C1 84.96(15), N4−Ta1−C1 77.84(15), C5−N3−Ta1 79.6(2), N3−C5−Ta1 60.8(2).

Scheme 6. Deuterium Labeling Study in the Synthesis of d_3-**13**

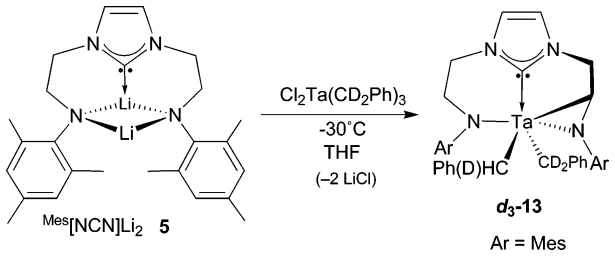

would yield d_4-**13** with two $-CD_2Ph$ groups, and no benzylic protio resonances would be observed. The reaction of **5** with $Cl_2Ta(CD_2Ph)_3$ yields d_3-**13**. The ^{1}H NMR spectrum clearly shows a 1:1:1 triplet at 2.70, evidence of a Ta*CH*(D)Ph resonance. This evidence corroborates the DFT calculations and supports the premise that the decomposition of [NCN]Ta(alkyl)$_3$ complexes proceeds through an alkylidene intermediate that rapidly undergoes endocyclic C−H bond activation with an amido donor arm.

Conclusions

In this work, we have examined the potential of the [NCN] ligand architecture to stabilize tantalum amide, halide, and alkyl complexes. Protonolysis protocols via aminolysis and alkyl elimination reactions, which were previously successful in the synthesis of group 4 [NCN] complexes, provide a route to incorporate one flanking amido arm only for the less sterically hindered ligand precursor, $^{p-Tol}$[NCN]H$_2$. Unfortunately, attempts to promote coordination of the second pendent amine arm have so far been unsuccessful. However, coordination of both pendent amide donors was achieved by metathesis reactions between ^{R}[NCN]Li$_2$ and substituted tantalum chlorides. In the case of trialkyldichlorotantalum(V) derivatives, endocyclic C−H bond activation of one of the amido backbone arms occurs rapidly to generate a new cyclometalated metallaaziridine. DFT

calculations on model complexes support the observation that these endocyclic products are thermodynamically favored over the unobserved trialkyl derivatives. More importantly, the computational results are consistent with the intermediacy of a tantalum alkylidene intermediate, which can then mediate C−H bond activation with a neighboring backbone linker C−H group to form a new metallaaziridine. In light of these findings, we attempted to synthesize a tantalum alkylidene complex stabilized by an [NCN] ancillary ligand and found that identical amide C−H bond activation occurs. While this result alone cannot confirm the mechanism postulated by DFT calculations, deuterium-labeling experiments are consistent with the involvement of a tantalum alkylidene intermediate during this process.

Computational studies of the electronic structure of early metal NHC complexes are rare and little more than cursory in their analysis.[46−49] Herein, we have studied the Ta−NHC interaction by DFT in detail and have discovered that the observed shortening of the Ta−carbene bond distance is a result of the formation of the metallaaziridine, which allows the NHC and the methyl substituents to adopt preferable bonding positions.

We are currently exploring the modification of the [NCN] ligand architecture to prevent amide C−H bond activation with a goal that these modified ligand−metal complexes will aid in small molecule activation and new catalytic processes by early metal derivatives.

Experimental Section

General Considerations. Unless otherwise stated, all manipulations were performed under an atmosphere of dry oxygen-free argon or nitrogen by means of standard Schlenk or glovebox techniques. Ta(NMe$_2$)$_5$ was purchased from Strem Chemicals and used as received. All other chemicals were purchased from Aldrich and used as received. ^{Mes}[NCN]H$_2$ (**1**),[18] $^{p-Tol}$[NCN]H$_2$ (**2**),[17] Ta(CH$_2$Ph)$_5$,[50] Cl$_2$Ta(NMe$_2$)$_3$,[24] Cl$_3$Ta(NMe$_2$)$_2$(THF),[51] Cl$_4$Ta(NEt$_2$)(Et$_2$O),[51] Cl$_2$TaMe$_3$,[52] Cl$_2$Ta(CH$_2$Ph)$_3$,[53] Cl$_2$Ta(CD$_2$Ph)$_3$,[53] Cl$_2$Ta(CH$_2$^{t}Bu)$_3$,[54] and Cl$_3$Ta=CH^{t}Bu(THF)$_2$[55] were synthesized by literature methods. Hexanes, toluene, and tetrahydrofuran were purchased anhydrous from Aldrich, sparged with nitrogen, and passed through columns containing activated alumina and Ridox catalyst. C$_6$D$_6$, CD$_3$C$_6$D$_5$, and C$_5$D$_5$N were dried by refluxing with sodium/potassium alloy in a sealed vessel under partial pressure, then trap-to-trap distilled, and freeze−pump−dethawed several times. ^{1}H and ^{13}C NMR spectra were recorded on a Bruker AVANCE 400 instrument operating at 400.0 MHz for ^{1}H. Elemental analyses, IR spectroscopy, and mass spectrometry (EI/MS) were performed at the Department of Chemistry at the University of British Columbia.

Synthesis of $^{p-Tol}$[NCNH]Ta(NMe$_2$)$_4$ (3). To a stirred solution of Ta(NMe$_2$)$_5$ (216 mg, 0.54 mmol) in toluene (5 mL) was added a toluene solution (5 mL) of **2** (181 mg, 0.54 mmol). The orange mixture was stirred overnight and filtered through Celite. The solvent was removed until the volume was ∼5 mL, and then cooled to −30 °C to yield orange blocks (66%). ^{1}H NMR (C$_6$D$_6$, 400 MHz): δ 2.22 (s, 3H, −ArC*H*$_3$), 2.44 (s, 3H, −ArC*H*$_3$), 3.06 (br s, 12H, −NC*H*$_3$), 3.16 (m, 2H, −NC*H*$_2$), 3.27 (m, 2H, −NC*H*$_2$), 3.32 (br m, 1H, −N*H*), 3.52 (br s, 6H, −NC*H*$_3$), 3.75 (br s, 6H, −NC*H*$_2$), 4.03 (m, 2H, −NC*H*$_2$), 4.19 (m, 2H, −NC*H*$_2$), 5.98 (br s, 1H, −imid*H*), 6.29 (br s, 1H, −imid*H*), 6.38 (d, J = 7 Hz, 2H, −Ar*H*), 6.91 (d, J = 7 Hz, 2H, −Ar*H*), 7.01 (d, J = 7 Hz, 2H, −Ar*H*), 7.24 (d, J = 7 Hz, 2H, −Ar*H*). ^{13}C NMR (C$_6$D$_6$, 121 MHz): δ 18.1 (−*C*H$_3$), 20.2 (−*C*H$_3$), 45.5 (br, −NCH$_3$), 46.9 (−NCH$_2$), 47.0 (−NCH$_2$), 47.5 (−NCH$_2$), 48.9 (−NCH$_2$), 118.6 (−Ar*C*), 119.3 (−Ar*C*), 120.5 (−imid*C*), 122.6 (−imid*C*), 124.8 (−Ar*C*), 124.9 (−Ar*C*), 128.7 (−Ar*C*), 129.2 (−Ar*C*), 140.5 (−Ar*C*), 141.6 (−Ar*C*), 198.5 (−N*C*N). Anal. Calcd for C$_{29}$H$_{49}$N$_8$Ta: C, 50.43; H, 7.15; N, 16.22. Found: C, 50.11; H, 7.00; N, 15.95.

Synthesis of ^{Mes}[NCNH]Ta=CHPh(CH$_2$Ph)$_2$ (4). To a stirred toluene solution (5 mL) of Ta(CH$_2$Ph)$_5$ (328 mg, 0.51 mmol) was added a toluene solution (5 mL) of **1** (200 mg, 0.51 mmol). The dark brown mixture was stirred overnight and filtered through Celite. The solvent was removed to yield a brown residue, which was triturated with hexanes to yield a brown powder (76% yield). X-ray quality crystals were obtained from a cooled (−30 °C) toluene solution. ^{1}H NMR (C$_6$D$_6$, 400 MHz): δ 2.02 (s, 3H, -*p*-ArC*H*$_3$), 2.08 (s, 6H, -*o*-ArC*H*$_3$), 2.20 (s, 6H, -*o*-ArC*H*$_3$), 2.31 (s, 3H, -*p*-ArC*H*$_3$), 2.42 (m, 4H, −TaC*H*$_2$), 2.43−3.10 (m, 7H, −N*H* and −NC*H*$_2$) and 3.58 (dt, J = 6 Hz, 1H, −NC*H*), 4.40 (dt, J = 6 Hz, 1H, −NC*H*), 4.81 (s, 1H, −C*H*Ph), 5.81 (d, J = 2 Hz, 1H, −imid*H*), 6.23 (d, J = 2 Hz, 1H, −imid*H*), 6.60−6.85 (m, H, −Ar*H*), 7.42 (d, J = 8 Hz, 4H, −Ar*H*). ^{13}C NMR (C$_6$D$_6$, 121 MHz): δ 17.9 (−*C*H$_3$), 18.2 (−*C*H$_3$), 20.7 (−*C*H$_3$), 21.0 (−*C*H$_3$), 48.7 (−NCH$_2$), 48.8 (−NCH$_2$), 51.6 (−NCH$_2$), 54.5 (−NCH$_2$), 69.9 (−TaCH$_2$), 85.0 (−TaCH$_2$), 119.6 (−Ar*C*), 120.3 (−Ar*C*), 121.2 (−imid*C*), 123.7 (−imid*C*), 125.6 (−Ar*C*), 129.3 (−Ar*C*), 129.8 (−Ar*C*), 129.9 (−Ar*C*), 130.6 (−Ar*C*), 131.0 (−Ar*C*), 132.0 (−Ar*C*), 136.1 (−Ar*C*), 137.6 (−Ar*C*), 137.8 (−Ar*C*), 138.2 (−Ar*C*), 142.7 (−Ar*C*), 147.8 (−Ar*C*), 148.7 (−Ar*C*), 155.3 (−Ar*C*), 205.0 (−N*C*N), 236.3 (−Ta*C*H). Anal. Calcd for C$_{46}$H$_{53}$N$_4$Ta: C, 65.55; H, 6.34; N, 6.65. Found: C, 65.26; H, 6.22; N, 65.95.

Synthesis of ^{Mes}[NCN]Li$_2$ (5), $^{p-Tol}$[NCN]Li$_2$ (6). The following procedure is representative of the synthesis of both **5** and **6**. A toluene solution (5 mL) of **5** (530 mg, 1.6 mmol) was cooled to −30 °C, and 1.0 mL of 1.6 M BuLi (1.6 mmol) was added slowly dropwise. The solution immediately darkened after the first equivalent was added, and a white precipitate formed after addition of the second equivalent of base was complete. The white suspension was allowed to warm slowly to room temperature and then stirred overnight. Filtration, followed by washing with several portions of toluene, yields a white powder (∼99% yield). **5**, ^{1}H NMR (C$_5$H$_5$N, 400 MHz): δ 2.35 (s, 6H, -*p*-ArC*H*$_3$), 2.46 (s, 6H, -*o*-ArC*H*$_3$), 4.08 (m, 4H, −NC*H*$_2$), 4.18 (m, 4H, −NC*H*$_2$), 6.81 (s, 4H, −Ar*H*), 6.91 (s, 2H, −imid*H*). ^{13}C NMR (C$_5$H$_5$N, 121 MHz): δ 20.4 (−*C*H$_3$), 21.3 (−*C*H$_3$), 46.8 (−NCH$_2$), 47.8 (−NCH$_2$), 119.5 (−Ar*C*), 119.9 (−Ar*C*), 123.6 (−imid*C*), 127.9 (−Ar*C*), 149.5 (−Ar*C*), 190.2 (−N*C*N). ^{7}Li NMR (C$_5$H$_5$N, 155 MHz): δ 2.88. Anal. Calcd for C$_{25}$H$_{32}$Li$_2$N$_4$: C, 74.61; H, 8.01; N, 13.92. Found: C, 74.55; H, 7.95; N, 13.86. **6**, ^{1}H NMR (C$_5$H$_5$N, 400 MHz): δ 2.29 (s, 6H, −ArC*H*$_3$), 3.62 (m, 4H, −NC*H*$_2$), 4.13 (m, 4H, −NC*H*$_2$), 6.69 (s, 4H, −Ar*H*), 7.00 (s, 2H, −imid*H*). ^{13}C NMR (C$_5$H$_5$N, 121 MHz): δ 21.4 (−*C*H$_3$), 45.6 (−NCH$_2$), 47.2 (−NCH$_2$), 117.9 (−Ar*C*), 120.5 (−Ar*C*), 122.9 (−imid*C*), 126.9 (−Ar*C*), 148.6 (−Ar*C*), 189.9 (−N*C*N). ^{7}Li NMR (C$_5$H$_5$N, 155 MHz): δ 2.86. Anal. Calcd for C$_{21}$H$_{24}$Li$_2$N$_4$: C, 72.83; H, 6.98; N, 16.18. Found: C, 72.79; H, 6.78; N, 16.01.

Synthesis of $^{p-Tol}$[NCN]Ta(NMe$_2$)$_3$ (7), $^{p-Tol}$[NCN]Ta(NMe$_2$)$_2$Cl (8), and $^{p-Tol}$[NCN]Ta(NEt$_2$)Cl$_2$ (9,10). The following procedure is representative of the synthesis of **7**−**10**. To a cooled (−30 °C) THF solution (5 mL) of Cl$_2$Ta(NMe$_2$)$_3$ (288 mg, 0.75 mmol) was added a chilled (−30 °C) THF solution (5 mL) of **5** (408 mg, 0.75 mmol). The mixture slowly darkens to brown upon warming to room temperature.

(46) Niehues, M.; Kehr, G.; Erker, G.; Birgit, W.; Fröhlich, R.; Blacque, O.; Berke, H. *J. Organomet. Chem.* **2002**, *663*, 192.
(47) Niehues, M.; Erker, G.; Kehr, G.; Schwab, P.; Fröhlich, R.; Blacque, O.; Berke, H. *Organometallics* **2002**, *21*, 2905.
(48) Abernathy, C. D.; Codd, G. M.; Spicer, M. D.; Taylor, M. K. *J. Am. Chem. Soc.* **2003**, *125*, 1128.
(49) Mungur, S. A.; Blake, A. J.; Wilson, C.; McMaster, J.; Arnold, P. A. *Organometallics* **2006**, *25*, 1861.
(50) Groysman, S.; Goldberg, I.; Kol, M.; Goldschmidt, Z. *Organometallics* **2003**, *22*, 3793.
(51) Chao, Y. W.; Polson, S.; Wigley, D. E. *Polyhedron* **1990**, *9*, 2709.
(52) Schrock, R. R.; Sharp, P. R. *J. Am. Chem. Soc.* **1978**, *100*, 2389.
(53) Schrock, R. R. *J. Organomet. Chem.* **1976**, *122*, 209.
(54) Li, L.; Diminnie, J. B.; Liu, X.; Pollitte, J. L.; Xue, Z. *Organometallics* **1996**, *15*, 3520.
(55) Boncella, J. M.; Cajigal, M. L.; Abboud, K. A. *Organometallics* **1996**, *15*, 1905.

After being stirred overnight, the solvent was removed and toluene (10 mL) was added. The solution was filtered through Celite, and the solvent was removed to yield an orange/brown residue. Trituration of the residue with hexane yielded an orange solid, which was recrystallized from toluene. **7**, ^{1}H NMR (C_6D_6, 400 MHz): δ 2.45 (s, 6H, −ArCH_3), 3.22 (s, 12H, −NCH_3), 3.53 (m, 4H, −NCH_2), 3.68 (s, 6H, NCH_3), 4.15 (m, 4H, −NCH_2), 6.00 (s, 2H, −imid*H*), 7.11 (d, J = 8 Hz, 4H, −Ar*H*), 7.27 (d, J = 8 Hz, 4H, −Ar*H*). ^{13}C NMR (C_6D_6, 121 MHz): δ 18.7 (−*C*H$_3$), 45.4 (−N*C*H$_3$), 47.0 (−N*C*H$_3$), 48.0 (−N*C*H$_2$), 50.7 (−N*C*H$_2$), 117.3 (−Ar*C*), 118.3 (−Ar*C*), 124.4 (−imid*C*), 126.6 (−Ar*C*), 152.6 (−Ar*C*), 186.7 (−N*C*N). Anal. Calcd for $C_{27}H_{42}N_7Ta$: C, 50.23; H, 6.56; N, 15.19. Found: C, 50.10; H, 6.35; N, 15.05. **8**, ^{1}H NMR (C_6D_6, 400 MHz): δ 2.26 (s, 6H, −ArCH_3), 3.26 (s, 6H, −NCH_3), 3.36 (m, 2H, −NC*H*H), 3.60 (m, 2H, −NC*H*H), 3.80 (s, 6H, −NCH_3), 3.88 (m, 2H, −NC*H*H), 4.35 (m, 2H, −NC*H*H), 5.96 (s, 2H, −imid*H*), 7.10 (d, J = 8 Hz, 4H, −Ar*H*), 7.36, 7.10 (d, J = 8 Hz, 4H, −Ar*H*). ^{13}C NMR (C_6D_6, 121 MHz): δ 19.5 (−*C*H$_3$), 45.6 (−N*C*H$_3$), 46.5 (−N*C*H$_3$), 47.5 (−N*C*H$_2$), 48.9 (−N*C*H$_2$), 116.8 (−Ar*C*), 119.1 (−Ar*C*), 123.9 (−imid*C*), 127.5 (−Ar*C*), 149.9 (−Ar*C*), 187.1 (−N*C*N). Anal. Calcd for $C_{25}H_{36}ClN_6Ta$: C, 47.14; H, 5.70; N, 13.19. Found: C, 47.09; H, 5.52; N, 12.95. Minor isomer (**9**), ^{1}H NMR (C_6D_6, 400 MHz): δ 0.60 (t, J = 9 Hz, 6H, −N(CH$_2$CH_3)$_2$), 2.28 (s, 6H, −ArCH_3), 3.25 (m, 2H, −NC*H*H), 3.52 (m, 2H, −NC*H*H), 3.56 (q, J = 9 Hz, 4H, −N(CH_2CH$_3$)$_2$), 3.98 (m, 2H, −NC*H*H), 4.70 (m, 2H, −NC*H*H), 6.10 (s, 2H, −imid*H*), 7.17 (d, J = 8 Hz, 4H, −Ar*H*), 7.61 (d, J = 8 Hz, 4H, −Ar*H*). ^{13}C NMR (C_6D_6, 121 MHz): δ 15.0 (−NCH$_2$*C*H$_3$), 22.5 (−*C*H$_3$), 45.4 (−N*C*H$_2$CH$_3$), 48.0 (−N*C*H$_2$), 50.7 (−N*C*H$_2$), 119.5 (−Ar*C*), 120.5 (−Ar*C*), 125.6 (−imid*C*), 131.5 (−Ar*C*), 151.6 (−Ar*C*), 189.5 (−N*C*N). Major isomer (**10**), ^{1}H NMR (C_6D_6, 400 MHz): 0.81 (t, J = 9 Hz, 6H, −N(CH$_2$CH_3)$_2$), 2.21 (s, 6H, −ArCH_3), 3.30 (m, 4H, −NCH_2), 3.74 (q, J = 9 Hz, 4H, −N(CH_2-CH$_3$)$_2$), 4.52 (m, 4H, −NCH_2), 5.78 (s, 2H, −imid*H*), 7.02 (d, J = 8 Hz, 4H, −Ar*H*), 7.49 (d, J = 8 Hz, 4H, −Ar*H*). ^{13}C NMR (C_6D_6, 121 MHz): δ 15.2 (−NCH$_2$*C*H$_3$), 23.4 (−*C*H$_3$), 45.9 (−N*C*H$_2$CH$_3$), 48.6 (−N*C*H$_2$), 51.6 (−N*C*H$_2$), 117.6 (−Ar*C*), 120.9 (−Ar*C*), 126.8 (−imid*C*), 132.6 (−Ar*C*), 153.9 (−Ar*C*), 185.6 (−N*C*N). Anal. Calcd for $C_{25}H_{34}Cl_2N_5Ta$: C, 45.74; H, 5.22; N, 10.67. Found: C, 45.45; H, 5.01; N, 10.52. Ratio of minor isomer **9**:major isomer **10** = 1:1.3.

Synthesis of ^{Mes}[NCCN]Ta(CH$_2$^{t}Bu)$_2$ (11), ^{Mes}[NCCN]TaMe$_2$ (12), ^{Mes}[NCCN]Ta(CH$_2$Ph)$_2$ (13), and ^{Mes}[NCCN]Ta(CD$_2$Ph)$_2$ (d_3-13). The following procedure is representative of the synthesis of **11**−**13**. To a cooled (−30 °C) THF solution (5 mL) of Cl$_2$Ta(CH$_2$^{t}Bu)$_3$ (360 mg, 0.77 mmol) was added a chilled (−30 °C) THF solution (5 mL) of **5** (270 mg, 0.77 mmol). The dark brown mixture was slowly warmed to room temperature. After being stirred overnight, the solvent was removed and toluene was added. The solution was filtered through Celite, and the solvent was removed to yield a dark orange solid (68% yield). Yellow crystals could be obtained by recrystallization from hexane. **11**, ^{1}H NMR (C_6D_6, 400 MHz): δ 0.80 (d, J = 8 Hz, 1H, −TaC*H*H), 0.92 (s, 9H, −C(CH_3)$_3$), 1.10 (d, J = 8 Hz, 1H, −TaC*H*H), 1.18 (d, J = 8 Hz, 1H, −TaC*H*H), 1.29 (d, J = 8 Hz, 1H, −TaC*H*H), 1.30 (s, 9H, −C(CH_3)$_3$), 2.18 (s, 3H, −ArCH_3), 2.25 (s, 3H, −ArCH_3), 2.28 (s, 3H, −ArCH_3), 2.67 (m, 1H, −NC*H*H), 2.86 (s, 3H, −ArCH_3), 3.60 (m, 1H, −NC*H*H), 3.67 (m, 1H, −NC*H*H), 3.84 (m, 2H, −NC*H*H), 4.34 (m, 1H, −NC*H*H), 4.48 (m, 1H, −NC*H*H), 5.82 (d, J = 2 Hz, 1H, −imid*H*), 5.88 (d, J = 2 Hz, 1H, −imid*H*), 6.80 (br s, 2H, −Ar*H*), 7.05 (s, 1H, −Ar*H*), 7.14 (s, 1H, −Ar*H*). ^{13}C NMR (C_6D_6, 121 MHz): δ 18.8 (−*C*H$_3$), 19.2 (−*C*H$_3$), 20.5 (−*C*H$_3$), 21.9 (−*C*H$_3$), 22.9 (−*C*H$_3$), 35.1 (−*C*(CH$_3$)), 36.0 (−*C*(CH$_3$)), 51.2 (−N*C*H$_2$), 55.9 (−N*C*H$_2$), 56.3 (−N*C*H$_2$), 68.1 (−Ta*C*), 72.1 (−Ta*C*), 85.6 (−Ta*C*), 117.5 (−Ar*C*), 119.5 (−Ar*C*), 120.5 (−imid*C*), 121.6 (−imid*C*), 129.6 (−Ar*C*), 130.9 (−Ar*C*), 132.1 (−Ar*C*), 133.9 (−Ar*C*), 148.6 (−Ar*C*), 149.9 (−Ar*C*), 197.5 (−N*C*N). Anal. Calcd for $C_{33}H_{47}N_4Ta$: C, 59.14; H, 7.52; N, 7.88. Found: C, 58.95; H, 7.26; N, 7.59. **12**, ^{1}H NMR (C_6D_6, 400 MHz): δ 0.46 (s, 3H, −TaCH_3), 0.62 (s, 3H, −TaCH_3), 1.89 (s, 3H, −ArCH_3), 2.21 (s, 3H, −ArCH_3), 2.27 (s, 3H, −ArCH_3), 2.70 (s, 3H, −ArCH_3), 2.72 (m, 1H, −NC*H*H), 3.31 (m, 1H, −NC*H*H), 3.49 (m, 1H, −NC*H*H), 3.71 (m, 1H, −NC*H*H), 3.86 (m, 1H, −NC*H*H), 4.19 (m, 1H, −NC*H*H), 4.37 (m, 1H, −NC*H*H), 5.91 (d, J = 2 Hz, 1H, −imid*H*), 5.94 (d, J = 2 Hz, 1H, −imid*H*), 6.84 (br s, 2H, −Ar*H*), 7.02 (s, 1H, −Ar*H*), 7.09 (s, 1H, −Ar*H*). A satisfactory ^{13}C NMR spectrum and elemental analysis could not be obtained due to the sensitivity of this product. **13**, ^{1}H NMR (C_6D_6, 400 MHz): δ 1.67 (d, J = 7 Hz, −TaC*H*H), 2.27 (s, 3H, −ArCH_3), 2.29 (s, 3H, −ArCH_3), 2.32 (s, 3H, −ArCH_3), 2.45 (d, J = 7 Hz, −TaC*H*H), 2.61 (d, J = 7 Hz, −TaC*H*H), 2.76 (s, 3H, −ArCH_3), 2.82 (d, J = 7 Hz, −TaC*H*H), 3.28 (m, 1H, −TaC*H*H), 3.45 (m, 1H, −TaC*H*H), 3.55 (m, 1H, −TaC*H*H), 3.88 (m, 1H, −TaC*H*H), 4.12 (m, 1H, −TaC*H*H), 4.55 (m, 1H, −TaC*H*H), 5.90 (d, J = 2 Hz, 1H, −imid*H*), 5.92 (d, J = 2 Hz, 1H, −imid*H*), 6.64−6.71 (m, 3H, −Ar*H*), 6.81−6.93 (m, 6H, −Ar*H*), 6.99−7.17 (m, 7H, −Ar*H*). ^{13}C NMR (C_6D_6, 121 MHz): δ 17.6 (−*C*H$_3$), 18.9 (−*C*H$_3$), 19.6 (−*C*H$_3$), 20.5 (−*C*H$_3$), 50.1 (−N*C*H$_2$), 54.6 (−N*C*H$_2$), 55.4 (−N*C*H$_2$), 79.2 (−Ta*C*), 81.6 (−Ta*C*), 90.1 (−Ta*C*), 119.2 (−Ar*C*), 120.2 (−imid*C*), 121.9 (−Ar*C*), 122.3 (−imid*C*), 124.6 (−Ar*C*), 124.9 (−Ar*C*), 129.6 (−Ar*C*), 130.6 (−Ar*C*), 131.5 (−Ar*C*), 135.6 (−Ar*C*), 145.6 (−Ar*C*), 148.6 (−Ar*C*), 149.6 (−Ar*C*), 151.2 (−Ar*C*), 196.2 (−N*C*N). Some aryl resonances were obscured by solvent signals. Anal. Calcd for $C_{43}H_{41}N_4Ta$: C, 62.39; H, 6.04; N, 7.46. Found: C, 61.98; H, 5.89; N, 7.19. d_3-**13**, ^{1}H NMR (C_6D_6, 400 MHz): NMR is identical to **13** with the absence of the peaks at ppm and ppm and the presence at δ 2.70 (t, $^2J_{HD}$ = 11 Hz, 1H, −TaC*H*D).

Synthesis of ^{Mes}[NCCN]Ta(CH$_2$^{t}Bu)Cl (14). To a cooled (−30 °C) THF solution (5 mL) of Cl$_3$Ta=CH(^{t}Bu)(THF)$_2$ (311 mg, 0.62 mmol) was added a chilled (−30 °C) THF solution (5 mL) of **5** (249 mg, 0.62 mmol). The dark brown mixture was slowly warmed to room temperature. After being stirred overnight, the solvent was removed and toluene added. The solution was filtered through Celite, and the solvent was removed to yield a dark orange solid (84% yield). Yellow crystals could be obtained by recrystallization from hexane. ^{1}H NMR ($CD_3C_6D_5$, 400 MHz): δ 1.26 (s, 9H, −C(CH_3)$_3$), 1.93 (d, J = 12 Hz, 1H, −TaC*H*H), 2.10 (s, 3H, −ArCH_3), 2.12 (s, 3H, −ArCH_3), 2.21 (d, J = 12 Hz, 1H, −TaC*H*H), 2.24 (s, 3H, −ArCH_3), 2.73 (s, 3H, −ArCH_3), 2.91 (m, 1H, −NC*H*H), 3.13 (m, 1H, −NC*H*H), 3.60 (m, 1H, −NC*H*H), 3.83 (m, 2H, −NC*H*H), 3.96 (m, 1H, −NC*H*H), 4.42 (m, 1H, −NC*H*H), 5.82 (br s, 1H, −imid*H*), 5.85 (br s, 1H, −imid*H*), 6.60 (s, 1H, −Ar*H*), 6.87 (s, 2H, −Ar*H*), 7.01 (s, 1H, −Ar*H*). ^{13}C NMR ($CD_3C_6D_5$, 121 MHz): δ 19.1 (−*C*H$_3$), 20.1 (−*C*H$_3$), 21.1 (−*C*H$_3$), 21.9 (−*C*H$_3$), 36.1 (−*C*(CH$_3$)), 52.0 (−N*C*H$_2$), 54.6 (−N*C*H$_2$), 57.2 (−N*C*H$_2$), 75.2 (−Ta*C*), 83.3 (−Ta*C*), 116.9 (−Ar*C*), 121.5 (−imid*C*), 122.8 (−imid*C*), 132.0 (−Ar*C*), 134.2 (−Ar*C*), 136.2 (−Ar*C*), 138.6 (−Ar*C*), 150.6 (−Ar*C*), 150.8 (−Ar*C*), 196.3 (−N*C*N). Anal. Calcd for $C_{29}H_{39}ClN_4Ta$: C, 53.37; H, 6.27; Cl, 5.25; N, 8.30. Found: C, 53.05; H, 6.02; Cl, ; N, 8.220.

Theoretical Calculations. All calculations were performed using the Gaussian 03 suite of programs.[56] Optimized gas-phase geometries were obtained using the Becke3 exchange functional,[57] in combination with the Lee, Yang, and Parr correlation functional,[58] that is, the B3LYP method, as implemented in Gaussian 03. The basis set (BS1) used for geometry optimizations and energy calculations was implemented as follows: for tantalum, the valence double-ζ LANL2DZ[59−61] basis set was supplemented with a set of 6p functions for transition metals developed by Couty and Hall,[62] while for all hydrogen, carbon, and nitrogen atoms, the 6-31G(d′,p′) basis sets[63−68] were used. All structures

(56) Frisch, M. J.; et al. *Gaussian 03*, revision B.4; Gaussian, Inc.: Pittsburgh, PA, 2003.
(57) Becke, A. D. *J. Chem. Phys.* **1993**, *98*, 5648.
(58) Lee, C.; Yang, W.; Parr, R. G. *Phys. Rev. B: Condens. Matter Mater. Phys.* **1988**, *37*, 785.
(59) Hay, P. J.; Wadt, W. R. *J. Chem. Phys.* **1985**, *82*, 270.
(60) Wadt, W. R.; Hay, P. J. *J. Chem. Phys.* **1985**, *82*, 284.
(61) Hay, P. J.; Wadt, W. R. *J. Chem. Phys.* **1985**, *82*, 299.
(62) Couty, M.; Hall, M. B. *J. Comput. Chem.* **1996**, *17*, 1359.
(63) Ditchfield, R.; Hehre, W. J.; Pople, J. A. *J. Chem. Phys.* **1971**, *54*, 724.

were calculated in singlet spin states using the restricted B3LYP method. Calculating the harmonic vibrational frequencies and noting the number of imaginary frequencies confirmed the nature of all intermediates (NImag = 0) and transition state structures (NImag = 1). All gas-phase relative free energies are reported in kcal mol^{-1}, with the energy of ^{H}[NCN]$TaMe_3$ (^{H}[NCN] = $(HNCH_2CH_2)_2N_2C_3H_2$), **A**, set to 0.0 kcal mol^{-1}. For the computational investigation, ^{H}[NCN] was used in place of the experimental ligands ($^{p-Tol}$[NCN] and ^{Mes}[NCN]) to reduce the computational demands, while still providing two amide donors and one *N*-heterocyclic carbene donor to the tantalum center. JIMP representations of the intermediates and transition states were created using the JIMP software program.[69] Natural Bond Orbitals (NBO) calculations were conducted with Gaussian NBO Version 3.1.[44,70−74]

(64) Hehre, W. J.; Ditchfield, R.; Pople, J. A. *J. Chem. Phys.* **1972**, *56*, 2257.
(65) Hariharan, P. C.; Pople, J. A. *Theor. Chim. Acta* **1973**, *28*, 213.
(66) Petersson, G. A.; Al-Laham, M. A. *J. Chem. Phys.* **1991**, *94*, 6081.
(67) Petersson, G. A.; Bennett, A.; Tensfeldt, T. G.; Al-Laham, M. A.; Shirley, W. A.; Mantzaris, J. *J. Chem. Phys.* **1988**, *89*, 2193.
(68) Foresman, J. B.; Frisch, Æ. *Exploring Chemistry with Electronic Structure Methods*, 2nd ed.; Gaussian, Inc.: Pittsburgh, PA; p 110. The 6-31G(d′,p′) basis set has the d polarization functions for C, N, O, and F taken from the 6-311G(d) basis set, instead of the original arbitrarily assigned value of 0.8 used in the 6-31G(d) basis set.
(69) Manson, J.; Webster, C. E.; Hall, M. B. *JIMP Development*, version 0.1 (built for Windows PC and Redhat Linux 7.3); Department of Chemistry, Texas A& M University: College Station, TX, 2004; http://www.chem.tamu.edu/jimp/.
(70) Carpenter, J. E.; Weinhold, F. *J. Mol. Struct. (THEOCHEM)* **1988**, *169*, 41.
(71) Foster, J. P.; Weinhold, F. *J. Am. Chem. Soc.* **1980**, *102*, 7211.
(72) Reed, A. E.; Weinhold, F. *J. Chem. Phys.* **1983**, *83*, 1736.
(73) Reed, A. E.; Weinstock, R. B.; Weinhold, F. *J. Chem. Phys.* **1985**, *83*, 735.
(74) Reed, A. E.; Weinhold, F. *J. Chem. Phys.* **1985**, *83*, 1736.

Acknowledgment. M.D.F. and L.P.S. thank the NSERC of Canada for funding (Discovery Grant to M.D.F. and an NSERC PGS-B Scholarship to L.P.S.). M.B.H. and C.B. thank the NSF (CHE 0518074 and DMS 0216275) and the Welch Foundation (A-0648) for support.

Supporting Information Available: Information on X-ray data collection and processing for **3**, **4**, **7**, **11**, and **14**, and X-ray crystallographic data for **3**, **4**, **7**, **11**, and **14** (CIF); complete ref 56. This material is available free of charge via the Internet at http://pubs.acs.org.

JA063282X